Powder Technology 404 (2022) 117499

Contents lists available at ScienceDirect

Powder Technology

journal homepage: www.elsevier.com/locate/powtec

A novel method for convective drying rate estimation in a deep fixed porous material bed

Gediminas Skarbalius *, Algis Džiugys, Edgaras Misiulis, Robertas Navakas

Laboratory of Heat Equipment Research and Testing, Lithuanian Energy Institute, Breslaujos St. 3, LT-44403 Kaunas, Lithuania

ARTICLE INFO

Article history:
Received 2 September 2021
Received in revised form 18 March 2022
Accepted 9 May 2022
Available online 15 May 2022

Keywords:
Thermodynamics
Biomass
Fixed beds
Convective drying
Drying rate

ABSTRACT

In this paper, we propose a novel approach to describe the convective drying process of deep fixed porous material beds during the constant-rate drying period, which is based on the equation describing the heat power conservation within the drying zone. In addition, we propose a novel iterative method to solve the equation, which evaluates the outlet air temperature and the drying rate for the bed with given inlet air parameters. The validity of the proposed approach is examined against experimental and CFD numerical modelling data for two cases of biomass beds, namely, sawdust and barley grain, which represent typical porous material drying problems. Furthermore, the analysis of the conservation equation shows that the drying rate of the bed is proportional to the inlet air mass flow rate and is a function of the initial moisture content of the bed; however, it is independent of the bed volume.

1. Introduction

Over the last decades, the increasing global demand for energy has led to the excessive use of fossil fuels, releasing considerable amounts of greenhouse gases into the atmosphere, markedly affecting the environment. Therefore, the need for more environmentally neutral alternative energy sources is evident. One of these alternative fuel sources in a major energy sector (the heat and power generation sector) is woody biomass, which is renewable and nearly CO_2-neutral [1–3]. Today it accounts for approximately 14% of global energy use [4]. The main sources of woody biomass are forests, where the biomass is composed of all parts of the tree, and wood processing residuals, where the biomass is mainly composed of wood bark, sawdust and wood chips [5].

In recent years, the demand for biomass has risen; consequently, as there is a limited supply of high-quality biomass feedstock, the heat and power generation plants often resort to lower quality biomass [6]. The most important quality characteristic of biomass for thermochemical conversion is the moisture content. Inherently, biomass often has a high amount of moisture, owing to its bio-origin and its ability to absorb moisture from the environment. As a result, the biomass feedstock can contain moisture contents of up to 150 – 300% on a dry basis (d. b.), depending on the source [5,7,8]. Such high levels of moisture in biomass reduce the calorific value of the feedstock and complicates the thermal conversion processes employed in heat and power generation plants, because a considerable amount of energy is wasted to heat and evaporate the excessive moisture from the feedstock [9]. Furthermore, the incomplete conversion of biomass occurs when the moisture content exceeds a critical value, reducing the conversion efficiency and, if not properly addressed, increasing the emission of harmful gasses [5,10]. In addition, in cases when the wood biomass, as well as the municipal solid waste, is used for RDF (refuse-derived fuel) pellets production, the moisture content over 20% on a wet basis (w. b.) causes greater energy consumption required for the pelletisation process of biomass [11].

The common solution to reduce the moisture content of the biomass feedstock before conversion is to employ a forced convection deep fixed bed dryers [5]. The main controllable parameters of these dryers are the air temperature, air flow rate and feedstock height. Due to significant variations in the properties of the biomass feedstock, dryer parameters need be optimised on demand for specific working conditions, such as the biomass feedstock type, particle size distribution, initial moisture content, and preferred moisture content for conversion [12]. Optimisation of dryer parameters requires knowledge of the heat and mass transfer processes involved.

According to experimental studies [13–16], the convective drying process of deep fixed biomass beds (schematic representation given in Fig. 1 a) can be divided into three distinctive periods [17]: an initial warm-up period, a constant-rate drying period and one or more falling-rate periods (Fig. 1 d). In the initial warm-up period, the energy of the inlet air is consumed to heat and dry the porous material near the inlet of the bed (the drying zone formation) and to raise the temperature of the rest of the bed from the initial bed temperature $T_{b,0}$ to the

* Corresponding author.
E-mail addresses: gediminas.skarbalius@lei.lt (G. Skarbalius), algis.dziugys@lei.lt (A. Džiugys), edgaras.misiulis@lei.lt (E. Misiulis), robertas.navakas@lei.lt (R. Navakas).

https://doi.org/10.1016/j.powtec.2022.117499
0032-5910/

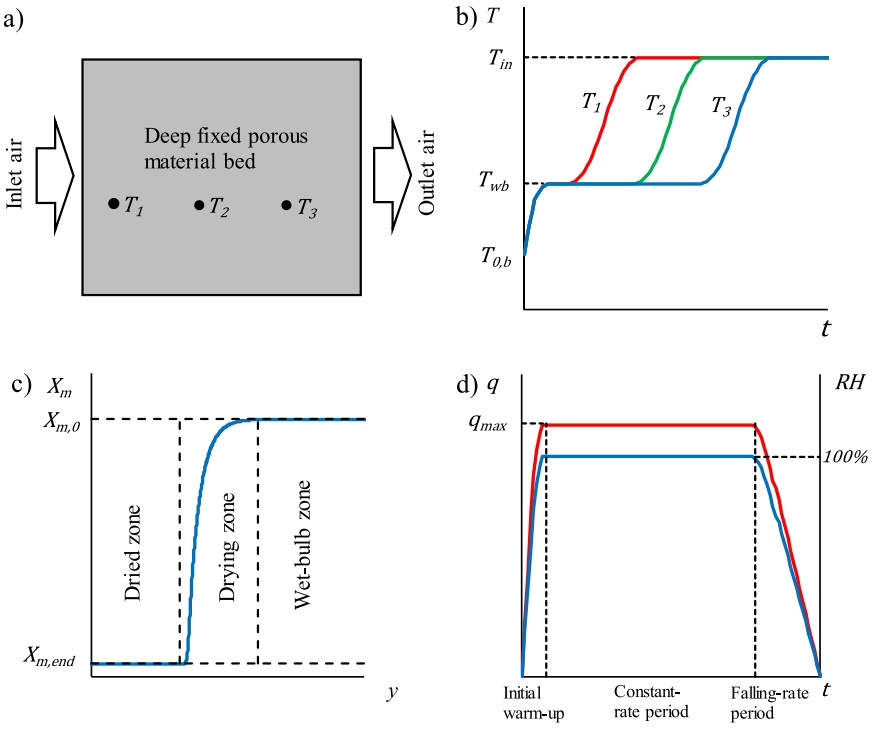

Fig. 1. a) Schematic representation of convective drying of a moist porous material bed; b) bed temperature evolution at three different bed positions; c) moisture content profile across the bed at specific time; d) drying rate evolution (left axis) and outlet air relative humidity revolution (right axis).

wet-bulb temperature T_{wb} [18] (Fig. 1 b). By the end of the warm-up period, the drying zone is fully formed, and the bed can be divided into three zones: the dried zone, drying zone and wet-bulb zone (Fig. 1 c). The drying zone here is considered as the spatial region of the bed where exchange of moisture from the wet material to the air takes place [14]. As the drying progresses into the constant-rate drying period, the drying zone starts to move downstream along the bed, leaving dried material behind, while the porous material beyond the drying zone still contains the same or slightly higher amount (due to condensation) of moisture as at the beginning of the drying process. Beyond the drying zone, the air is fully saturated with water vapour (relative humidity is 100%) and is in thermal equilibrium with the moist bed at the wet-bulb temperature T_{wb} (Fig. 1 b). Therefore, heat and mass transfer no longer take place as the saturated air continues to pass through the bed, and the outlet air temperature during the constant-rate drying period is equal to the wet-bulb temperature ($T_{out} = T_{wb}$). At the end of the drying process, the drying zone reaches the end of the bed, and the outlet air relative humidity, as well as the drying rate, start to decrease, while the outlet air temperature rises to the inlet air temperature (falling-rate drying period).

As the outlet air temperatures, at which the air reaches the relative humidity of 100% by absorbing the water vapour and losing its heat to the porous material, and the corresponding convective drying rates are not known in advance, many experimental studies have been performed on the drying process to understand the effects of different drying regimes on the drying conditions not only for woody biomass [6,16,19–28] but also for other drying problems, including drying of coal [29], food and fruit [30–36], textiles [37] and so on. Furthermore, a great number of mathematical models for simulating the drying process of deep beds with porous biological materials were proposed since 1950s [38,39]. Such models are based on the equilibrium of the moisture content with the environment and can be categorised as logarithmic, equilibrium and non-equilibrium models [40]. However, some degree of overlapping between different model categories exists and the classification is somewhat arbitrary. The logarithmic and equilibrium models are in general a form of a non-equilibrium models with simplifying assumptions to boundary conditions required to reduce the complexity and computational time [41].

The logarithmic drying models assume that the energy required for evaporating moisture from the wet porous material is equal to the change in enthalpy of the air passing through the material, which leads to a logarithmic relationships for drying parameters [39]. The logarithmic models are simple and computationally cheap; however, in most cases, their application has been limited to low temperature drying regimes of fixed porous material beds [42]. In both the equilibrium and non-equilibrium models, a system of differential equations is derived considering the heat and mass balance within the control volume [43]. In case of the equilibrium models, the thermal equilibrium between the drying air and wet porous material is assumed, which leads to a simplified system of differential equations describing the drying process. In contrary to equilibrium models, the equilibrium between drying air and porous material is not assumed in non-equilibrium models; thus, leading to more detailed and accurate description of the drying process. However, the non-equilibrium models are more demanding as their implementation requires numerical techniques based temporal and spatial discretization [44]. The extensive reviews on the classic drying models can be found in refs. [43,45–48]. In addition, as the computational power has been increasing over the last decades, more sophisticated and powerful computational tools based on the temporal and spatial discretisation of the process domain (such as CFD numerical simulations) have now replaced the classic models used for the numerical analysis of the drying processes [49]. The CFD numerical simulations method is capable of describing the drying process in high resolution; therefore, it has been used in number of studies to elucidate the drying experiments and predict the drying rate of various porous materials, for example, biomass [15,50–58].

In this paper, we propose a novel approach to describe the convective drying process of deep fixed porous material beds during the

constant-rate drying period, which is based on the equation describing the heat power conservation within the drying zone. In addition, we propose a simple and fast iterative method to solve the conservation equation since the equation cannot be solved analytically due to non-linear material property dependencies on temperature and the complex expressions of the equation terms. This method provides the possibility to evaluate the outlet air temperature and the corresponding convective drying rate of deep fixed porous material beds with given inlet air parameters without the need of sophisticated modelling techniques based on temporal or spatial discretisation of whole drying process and domain (such as CFD approaches). Furthermore, the validity of this approach is examined against experimental and CFD numerical modelling data for two cases of biomass beds, namely, sawdust and barley grain, which represent typical porous material drying problems. Notably, although the present work is concerned with deep fixed biomass bed drying scenarios, the method can be used to solve more general porous material convective drying problems with any type of evaporating liquids.

2. Materials and methods

The "Material and methods" section is navigated in the following way. First, the equation of heat power conservation that governs the drying process during the constant-rate period is introduced in Section 2.1. Then, the definitions for the conservation equation terms are given throughout Sections 2.2–2.5. Our proposed iterative method algorithm to solve the conservation equation is described in Section 2.6. The description of the experiments used to validate the iterative method is given in Section 2.7. The description for CFD numerical model that was used to supplement the validation and showcase some iterative method's limitations is given in Section 2.8. Finally, the thermal material properties used for both the iterative method and CFD numerical modelling are described in Section 2.9.

2.1. Equation of heat power conservation

In a deep fixed moist, porous material bed, a convective drying process can be described by the equation of heat power conservation within the drying zone during a constant rate-period. A deep fixed bed in this paper is regarded as a stationary porous material bed, in which the thickness of the fixed bed L_b is greater than the thickness of the drying zone L_{dz}. This condition has great importance because it ensures that during the constant-rate period the air beyond the drying zone is fully saturated with water vapour and is in thermal equilibrium with the moist bed at the wet-bulb temperature T_{wb}, which is also equal to the outlet air temperature $T_{out} = T_{wb}$ as described in introduction. In case this condition is not satisfied, the air is not able to reach saturation in the bed, and the presented approach becomes inapplicable.

During the constant-rate period, the drying zone slowly moves through the bed, and the heat power from the inlet air is consumed to evaporate the water. The materials such as woody biomass still contain residual water after drying [59]. The amount of residual water in dried biomass is determined by the final moisture content $X_{m,end}$, which is an equilibrium moisture content of biomass at inlet air conditions. The dried solid material and residual water are then heated up to inlet air temperature T_{in} within the drying zone. In the case of biomass, the equation of heat power conservation within the drying zone (independently of the drying zone thickness) which governs the drying process of the bed during the constant-rate period, is written as follows:

$$P_{in} = P_{evap} + P_{sorp} + P_s + P_{m,end} \tag{1}$$

where P_{in} is the heat power of inlet air, P_{evap} is the heat power consumed to evaporate water within the drying zone, P_{sorp} is the heat power used to break hydrogen bonds of sorbed water within the drying zone, P_s and $P_{m,end}$ are the heat power consumed to heat the dry solid (biomass) and the residual water inside the solid within the drying zone, respectively. These heat power terms during the constant-rate drying period are evaluated as follows.

2.2. Heat power of inlet air

As the material before the drying zone is already heated up to the inlet air temperature T_{in}, and the temperature beyond the drying zone is constant and equal to outlet air temperature T_{out} (which is equal to wet-bulb temperature $T_{out} = T_{wb}$), the heat power of the inlet air P_{in} is consumed within the drying zone. The heat power term P_{in} is defined as the energy that is transferred by the inlet air to moist solid when the air cools down from the inlet air temperature T_{in} to the outlet air temperature T_{out}. In many cases, the inlet air is a mixture of dry air and water vapour; therefore, P_{in} consists of two terms:

$$P_{in}(T_{in}, T_{out}) = \int_{T_{out}}^{T_{in}} c_{p,air}(T) q_{in,air} dT + \int_{T_{out}}^{T_{in}} c_{p,vap}(T) q_{in,vap} dT \tag{2}$$

where $c_{p,air}$ is the heat capacity of dry air ($J/(K \cdot kg)$), $c_{p,vap}$ is the heat capacity of water vapour ($J/(K \cdot kg)$), $q_{in,air}$ the inlet dry air mass flow rate (kg/s), and $q_{in,vap}$ is the inlet water vapour mass flow rate (kg/s). The total inlet air mass flow rate q_{in} is a sum of mass flow rates of dry air and water vapour:

$$q_{in} = q_{in,air} + q_{in,vap} \tag{3}$$

The mass flow rates $q_{in,air}$ and $q_{in,vap}$ are calculated from the experimentally measured inlet air volumetric flow rate Q_{in} (m^3/s), inlet air relative humidity RH_{in}, inlet air temperature T_{in} and inlet air pressure p_{in} as follows:

$$q_{in,air} = Q_{in} \rho_{in,air} \tag{4}$$

and

$$q_{in,vap} = Q_{in} \rho_{in,vap} \tag{5}$$

Since the water vapour pressure at the inlet is $p_{in,vap} = RH_{in} p_{sat,vap}(T_{in})$ ($p_{sat,vap}$ is the saturation pressure of water vapour), the density of dry air and water vapour at the inlet given by the ideal gas law are

$$\rho_{in,air} = \frac{p_{in,air} M_{air}}{R_g T_{out}} \tag{6}$$

and

$$\rho_{in,vap} = \frac{p_{in,vap} M_w}{R_g T_{in}} \tag{7}$$

here, $p_{in,air} = p_{in} - p_{in,vap}$ is the dry air pressure at the inlet, M_w is the molar mass of water (kg/mol), M_{air} is the molar mass of air (kg/mol), and R_g is the ideal gas constant ($J/(mol \cdot K)$).

2.3. The heat power of water evaporation

The heat power consumed for water evaporation for a given T_{out} is:

$$P_{evap}(T_{out}) = q_{evap}(T_{out}) h_{evap}(T_{out}) \tag{8}$$

where $h_{evap}(T_{out})$ is the latent heat of water evaporation at outlet air temperature T_{out} (J/kg). The drying rate is defined as a water mass-loss rate from the bed:

$$q_{evap}(T_{out}) = q_{out,vap}(T_{out}) - q_{in,vap} \tag{9}$$

where $q_{out,vap}(T_{out})$ is the outlet water vapour mass flow rate (kg/s). The mass flow rate $q_{out,vap}(T_{out})$ for given outlet air temperature T_{out}, pressure p_{out} and relative humidity RH_{out} can be evaluated as follows:

$$q_{out,vap}(T_{out}) = q_{out}(T_{out}) - q_{out,air} \tag{10}$$

where $q_{out,air}$ is the outlet dry air mass flow rate and is equal to $q_{in,air}$. The outlet air mass flow rate $q_{out}(T_{out})$ is calculated as:

$$q_{out}(T_{out}) = \frac{q_{out,air}}{\xi_{out,air}(T_{out})} \tag{11}$$

where $\xi_{out,air}$ is the mass fraction of dry air in outlet air:

$$\xi_{out,air}(T_{out}) = \frac{\rho_{out,air}(T_{out})}{\rho_{out,air}(T_{out}) + \rho_{out,vap}(T_{out})} \tag{12}$$

The density of water vapour and dry air at the outlet can be evaluated analogously to Eqs. (6) and (7):

$$\rho_{out,vap}(T_{out}) = \frac{p_{out,vap} M_w}{R_g T_{out}} \tag{13}$$

and

$$\rho_{out,air}(T_{out}) = \frac{\left(p_{out} - p_{out,vap}\right) M_{air}}{R_g T_{out}} \tag{14}$$

2.4. The heat power of sorption water evaporation

Since the wood is a hygroscopic material, additional energy is required to break the hydrogen bonds of bound water when the moisture content of wood is below the fibre saturation point $X_{m,fsp}$ during the drying process. This additional energy is a function of moisture content X_m (see Eq. (33)) and is accounted in heat power term P_{sorp}, which includes all additional energy required to dry the biomass from fibre saturation point $X_{m,fsp}$ to final moisture content $X_{m,end}$:

$$\begin{aligned} P_{sorp}(T_{out}) &= \int_{X_{m,end}}^{X_{m,fsp}} q_s 0.4 h_{evap}(T_{out}) \left(1 - X_m / X_{m,fsp}\right)^2 dX_m \\ &= q_s 0.4 h_{evap}(T_{out}) \frac{\left(X_{m,fsp} - X_{m,end}\right)^3}{3 X_{m,fsp}^2} \end{aligned} \tag{15}$$

Term q_s will be explained in the following section. The value of fibre saturation point of wood [60] is $X_{m,fsp} = 0.29$. The moisture content on dry basis X_m is defined as:

$$X_m(t) = m_w(t)/m_s(t) \tag{16}$$

where m_w is the mass of water in wet biomass (kg), and m_s is the mass of dry material in the bed (kg). The moisture content refers to moisture content on a dry basis throughout this paper. The mass of the dry material is constant during the drying process.

$$m_s(t) = const. \tag{17}$$

Consequently, $X_{m,0} = X_m(t = 0)$ is the initial moisture content, and $X_{m,end} = X_m(t = \infty)$ is the final moisture content after the drying process is completed.

2.5. The heat power of heating the solid and residual water

During the constant-rate drying period, when the drying zone moves through the bed, the ratio of q_{evap} to the mass rate of dried solid q_s is constant and equal to the difference between the initial and final moisture contents:

$$q_{evap}/q_s = X_{m,0} - X_{m,end} = const. \tag{18}$$

As the drying zone moves an infinitesimal distance during the drying, all water in the volume covered by the drying zone is evaporated, leaving the dried solid and the residual water, which are then heated from T_{out} to T_{in}. The rates at which the dry solid and the residual water are separated from the evaporating water can be interpreted as the mass rate of dry solid q_s and the mass rate of residual water $q_{m,end} = X_{m,end} q_s$, respectively. The heat power terms P_s and $P_{m,end}$, which are consumed for heating dry solid and residual moisture, are:

$$P_s(T_{in}, T_{out}) = \int_{T_{out}}^{T_{in}} c_{p,s}(T) q_s dT \tag{19}$$

and

$$P_{m,end}(T_{in}, T_{out}) = \int_{T_{out}}^{T_{in}} c_{p,w}(T) q_{m,end} dT \tag{20}$$

where $c_{p,s}$ is the heat capacity of dry solid ($J/(K \cdot kg)$), and $c_{p,w}$ is the heat capacity of liquid water ($J/(K \cdot kg)$).

2.6. The iterative method

The heat power terms in Eq. (1) are a function of the outlet air temperature T_{out}, which is unknown and cannot be estimated analytically from the conservation equation (Eq. (1)) owing to the complex expressions of the equation terms. However, here we show that T_{out}, and; consequently, the drying rate of the biomass bed $q_{evap}(T_{out})$ can be estimated by a iterative algorithm based on the same conservation of heat power equation given in Eq. (1). We would like to note again that saturated air and moist porous material beyond the drying zone are in thermal equilibrium at the wet-bulb temperature T_{wb}. Consequently, the temperature of saturated outlet air T_{out} is also equal to the wet-bulb temperature:

$$T_{out} = T_{wb} \tag{21}$$

The algorithm of the iterative method, which solves T_{out} and $q_{evap}(T_{out})$ is shown in Fig. 2. Before the iterations start, the drying conditions and material properties must be defined, which include:

- inlet conditions: Q_{in}, RH_{in}, T_{in}, p_{in} (and the required mass flow rates $q_{in,air}$ and $q_{in,vap}$, which are evaluated by Eqs. (4) and (5), respectively);
- outlet conditions: $RH_{out} = 1$, p_{out};
- air and biomass parameters and properties: $c_{p,s}(T)$, $c_{p,air}(T)$, $c_{p,vap}(T)$, $h_{evap}(T)$, $X_{m,0}$, $X_{m,end}(RH_{in})$.

Furthermore, we define the tolerance of the relative power disbalance ε_p and maximum number of iterations N_{max}, which are required to stop the iterations when the solution within the specified accuracy is reached, or the iteration number exceeds N_{max} to prevent infinite cycles.

In the case of liquid drying, the solution of T_{out} is in the range $(T_{freez}; T_{boil})$, where T_{freez} and T_{boil} are freezing and boiling temperatures of the liquid, respectively. Therefore, the initial lower and upper limits for T_{out} are

$$T_l^0 = T_{freez}, T_u^0 = T_{in} \tag{22}$$

We then guess the initial value of T_{out}:

$$T_{out}^0 = min\left(T_{boil} - \varepsilon_T, \frac{T_l^0 + T_u^0}{2}\right) \tag{23}$$

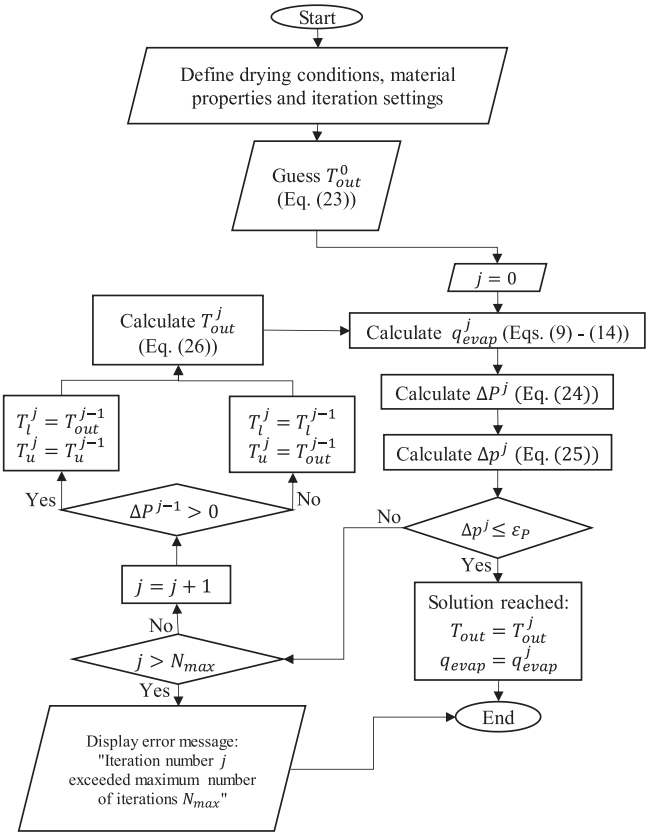

Fig. 2. Iterative method solution algorithm.

The T^0_{out} is guessed below boiling temperature T_{boil} to avoid instabilities in the solution algorithm solution, and ε_T is a small value ensuring that $T^0_{out} < T_{boil}$. For instance, $\varepsilon_T = 0.1\ K$.

After defining the initial iteration number $j = 0$, we calculate the evaporation rate $q^j_{evap}(T^j_{out})$ according to Eq. (9) and the heat power disbalance as follows

$$\Delta P^j = P^j_{in}\left(T_{in}, T^j_{out}\right) - \left[P^j_{evap}\left(T^j_{out}\right) + P^j_{sorp}\left(T^j_{out}\right) + P^j_{solid}\left(T_{in}, T^j_{out}\right) + P^j_{m,end}\left(T^j_{out}\right)\right] \quad (24)$$

for guessed temperature T^j_{out}. The terms P^j_{in}, P^j_{evap}, P^j_{sorp}, P^j_{solid} and $P^j_{m,end}$ are defined according to Eqs. (2), (8), (15), (19) and (20), respectively. At this point, if the relative heat power disbalance Δp^j defined as

$$\Delta p^j = \frac{\left|\Delta P^j\right|}{P^j_{in}\left(T_{in}, T^j_{out}\right)} \quad (25)$$

meets the condition $\Delta p^j \le \varepsilon_p$ (which means that required accuracy is reached), we stop the algorithm with the solution $T_{out} = T^j_{out}$ and $q_{evap} = q^j_{evap}$. Otherwise, if $\Delta p^j > \varepsilon_p$ and $j \le N_{max}$, we start new iteration $j = j + 1$, redefine the temperature limits T^j_l and T^j_u according to the sign of the ΔP^{j-1} and recalculate the guessed temperature for the $q^j_{evap}(T^j_{out})$ calculation in the new cycle as follows

$$T^j_{out} = \frac{\left(T^j_u + T^j_l\right)}{2} \quad (26)$$

It was empirically estimated that the number of iterations N required to reach the tolerance of the relative power disbalance $\varepsilon_P \ge \Delta p^j$ can be expressed as a logarithmic function of ε_P:

$$N \approx 1 - \frac{3}{2}\ ln\ (\varepsilon_P), N > 1 \quad (27)$$

The relative tolerance for drying rate estimation in this work was set to $\varepsilon_p = 1 \cdot 10^{-8}$, and the number of iterations required to reach the solution for sawdust and barley grain drying for method validation (Section 3.1) were 28 and 30, respectively.

Let us note that the presented iterative method has an advantage over other widely used methods to predict the drying rates, such as CFD methods because it is based on the equation of heat power conservation within the thin region of the bed (the drying zone). Therefore, the method does not require a temporal and spatial discretisation of the whole drying domain. Furthermore, the method does not require any additional software and can be implemented in any standard programming language, for example, in MATLAB/Octave.

2.7. Experimental procedure

The iterative method was validated by experimental data for two cases of biomass beds, namely, sawdust and barley, which represent a typical porous material drying problem.

In the sawdust drying experiment performed by Bengtsson [13], the sawdust was placed in a cylindrical drying chamber with a 0.4 *m* radius. The sawdust bed height was 0.42 *m*. The hot air supplied to the chamber from below with a centrifugal fan was heated to 57 ° *C*. The inlet air velocity was 0.25 *m/s*, and the relative humidity was 20%. The final moisture content $X_{m,end}$ was reported to be approximately 0.056.

In the barley drying experiment [19], the freshly harvested barley grain was dried in a cylindrical 1.37*m* diameter bin. The bed height was 2.2 *m*. The inlet air temperature was 25 ° *C*, and the relative humidity of inlet air was 67%. The initial and final moisture contents of the grain were 0.395 and 0.162, respectively. The initial temperature of the fixed barley grain bed was 15 ° *C*. The specific inlet air mass flow rate was 471 $kg/(m^2 \cdot h)$.

2.8. CFD numerical model

The CFD numerical modelling was performed with the same conditions as in the sawdust drying experiment described above to support the validation of the iterative method and showcase the method's limitations.

Here, a standard CFD numerical model considering the fluid flow through porous solid (biomass) was implemented in the COMSOL Multiphysics software [61]. The biomass was considered as a solid phase, while the moist air as fluid phase. Fluid flow momentum is governed by the standard modified incompressible Navier–Stokes equation formulation (Brinkman equation) in a porous medium [62]:

$$\frac{1}{\varepsilon}\rho_f \frac{\partial \mathbf{u_f}}{\partial t} + \frac{1}{\varepsilon}\rho_f (\mathbf{u_f} \cdot \nabla)\mathbf{u_f}\frac{1}{\varepsilon} = \nabla \cdot \left(-p\mathbf{I} + \mu_f \frac{1}{\varepsilon}\left(\nabla \mathbf{u_f} + (\nabla \mathbf{u_f})^{\mathrm{T}}\right)\right) - \left(\mu_f \kappa^{-1} + \beta_F |\mathbf{u_f}| + \frac{Q_m}{\varepsilon^2}\right)\mathbf{u} \quad (28)$$

where ε is the porosity of the solid phase; ρ, $\mathbf{u}$, μ and p are the density, velocity, viscosity and pressure, respectively; t is time; $\mathbf{I}$ is the identity matrix; κ is the permeability of the porous medium; β_F is the Forchheimer drag coefficient; and Q_m is the mass source due to water evaporation, which in this case is equal to the convective mass transport rate for water, $\dot{m}$. The subscript f denotes the fluid phase (dry air and vapour mixture).

The respective energy conservation equations for fluid and solid phases are:

$$\varepsilon\rho_f c_{p,f}\frac{\partial T_f}{\partial t}+\rho_f c_{p,f}\mathbf{u_f}\cdot\nabla T_f+\varepsilon\nabla\cdot\mathbf{q_f}=h_h A_{sf}(T_s-T_f) \tag{29}$$

and

$$(1-\varepsilon)\rho_s c_{p,s}\frac{\partial T_s}{\partial t}+\rho_s c_{p,s}\mathbf{u}_s\cdot\nabla T_s+(1-\varepsilon)\nabla\cdot\mathbf{q_s}= \dot{m}\,h_w+h_h A_{sf}(T_f-T_s) \tag{30}$$

where c_p is the specific heat, T is temperature, $\mathbf{q}=k\nabla T$ is the energy flux due to thermal conductivity, k is the thermal conductivity, h_h is the convective heat transfer coefficient, $\dot{m}$ is the convective mass transfer rate for water, A_{sf} is the specific surface area of biomass and h_w is the latent heat of water evaporation from biomass. The subscripts f and s denote fluid and solid phases, respectively. The specific surface area is defined as the fluid-solid contact surface area in unit volume and can be approximately evaluated by the following equation:

$$A_{sf}=\frac{\overline{A}_p}{\overline{V}_p}(1-\varepsilon) \tag{31}$$

where $\overline{A}_p$ is the average geometric surface area of the particle, $\overline{V}_p$ is the average geometric volume of the particle, and ε is the porosity. The sawdust particles in the sawdust experiment are considered as spheres with a diameter corresponding to the average size of the particles from a study [13]. Wood chip biomass is considered as the same material as sawdust but with different particle sizes and shapes. The average size of the wood chip particles for modelling was determined by measuring the size of a certain number of randomly selected wood chip particles [21]. The particles were idealized as rectangular prisms with average dimensions of $\overline{L}_p=(2.743,1.493,0.385)$ cm. The porosity value of the wood chip biomass with the same particle size distribution was obtained by DEM simulation of particle packing in a rectangular box (see Section 3.4). The obtained porosity value in the bulk region of the bed 0.28 is close to experimentally measured porosity values of wood chip beds given in ref. [63]. The intra-particle moisture and temperature are neglected in the numerical model.

The additional energy required for the bound water evaporation below fibre saturation point in biomass is accounted in the latent heat of water evaporation [64]:

$$h_w=h_{evap}+h_{sorp} \tag{32}$$

and

$$h_{sorp}=\begin{cases}0.4h_{evap}\left(1-\dfrac{X_m}{X_{m,fsp}}\right)^2 & when\ X_m\le X_{m,fsp}\\ 0 & when\ X_m>X_{m,fsp}\end{cases} \tag{33}$$

where h_{evap} is the latent heat of evaporation of water, X_m is the moisture content on a dry basis, and $X_{m,fsp}=0.29$ is the fibre saturation point [60].

Liquid water inside the biomass is transported only due to evaporation; by contrast, water vapour is transported by both diffusion and convection in addition to evaporation. The mass conservation equations for liquid water in the solid phase and water vapour in the fluid phase are:

$$\frac{\partial c_w}{\partial t}=-\dot{m} \tag{34}$$

and

$$\frac{\partial c_v}{\partial t}+\nabla\cdot(-D_v\nabla c_v)+\mathbf{u}_f c_v=\dot{m} \tag{35}$$

where c is the molar species concentration and D is a diffusivity constant. The subscripts w and v denote liquid water and water vapour, respectively. The convective mass transport rate for water $\dot{m}$ is given by:

$$\dot{m}=h_m A_{sf}(a_w c_{v,sat}-c_v) \tag{36}$$

where h_m is the convective mass transfer coefficient, $c_{v,sat}$ is the vapour saturation concentration, which is calculated for the solid phase temperature, and a_w is the water activity function for wood, which describes the equilibrium between moist wood and air (in the literature, it is often called the equilibrium moisture content curve). In this work, a_w is expressed as a function of the local moisture content and given by:

$$a_w=\frac{(a_{w,\,min}+a_{w,\,max})}{2}+\frac{(a_{w,\,min}-a_{w,\,max})}{2}\tanh\left(\frac{X_{m,a_w}-X_m}{\delta_{a_w}}\right) \tag{37}$$

The hyperbolic tangent function was chosen due to its resemblance to the water activity function shape [59]. The function coefficients $a_{w,min}=-0.051$, $a_{w,max}=1$, $X_{m,a_w}=0.097$ and $\delta_{a_w}=0.065$ were chosen in such way that the final moisture content would be close to the experimental value (see Fig. 3).

The convective heat and mass transfer coefficients are related by equation [32]:

$$h_m=\frac{h_h D_f}{k_f} \tag{38}$$

The convective heat transfer coefficient is given by:

$$h_h=\frac{Nu\cdot k_f}{\overline{d}_p} \tag{39}$$

where Nu is the Nusselt number and $\overline{d}_p$ is the average diameter of biomass particles. It was previously shown that the Nusselt number for a fixed bed of spherical and cylindrical particles is [65]:

$$Nu=1.77(\pm1.39)+0.29\varepsilon^{-0.81}Re^{0.73}Pr^{0.5} \tag{40}$$

when the porosity is in the range $0.405<\varepsilon<0.539$. The Reynolds number for a porous medium is given by:

$$Re=\frac{\rho_f\mathbf{u_f}\overline{d}_p}{\varepsilon\mu_f} \tag{41}$$

and the Prandtl number is given by:

$$Pr=\frac{c_{p,f}\mu_f}{k_f} \tag{42}$$

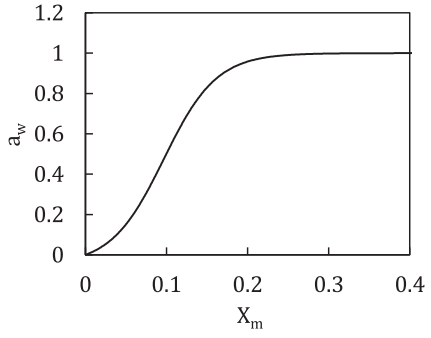

Fig. 3. Water activity function used in CFD numerical modelling for sawdust and wood chips.

Instead of modelling the whole 3D cylindrical drying chamber with a 0.4 m radius and a 0.42 m the bed height, we modelled a single 2D plane (plane dimensions 0.4x0.42 m) with axial symmetry boundary condition on the right boundary. On the left boundary (the chamber wall), a no-slip boundary condition was used for fluid phase flow, and no-flux conditions were used for heat transfer and mass transfer in both fluid and solid phases. The inlet was selected at the bottom boundary, and the outlet was selected at the top boundary. A standard COMSOL generated extra-fine quality mesh was used. The total number of mesh elements were around 371,000 with an average element inscribed diameter of 2.5 mm. The sawdust drying simulation results did not change when the quality of the mesh was further increased, which indicates that the quality of the mesh was sufficient. The same mesh quality and geometrical parameters (except the bed height) were used for wood chip biomass drying modelling in Section 3.3. Furthermore, in Section 3.4, the mesh quality in the regions with enlarged porosity was increased to accurately capture the flow redistribution due to enlarged porosity and its effects on drying.

The integration timestep was automatically controlled by COMSOL solver by maintaining the relative tolerance of $1 \cdot 10^{-3}$ and absolute tolerance of $1 \cdot 10^{-4}$.

2.9. Material thermal properties

In this section, we list the material thermal properties that were used for the iterative method and CFD numerical modelling. The tabulated data for the specific heat capacity of dry air $c_{p,air}$ [66] and the specific heat capacity of water vapour $c_{p,vap}$ [67] was approximated by a polynomial fits:

$$c_{p,air} = \sum_{i=1}^{N} a_{air,i} T^{i-1} \tag{43}$$

and

$$c_{p,vap} = \sum_{i=1}^{N} a_{vap,i} T^{i-1} \tag{44}$$

The unit of temperature used for the relations in this section is K. The specific heat capacity of dry wood $c_{p,wood}$ was defined according to ref. [59]:

$$c_{p,wood} = 103 + 3.867T \tag{45}$$

The heat capacity of barley grain was set as a constant value $c_{p,solid} = 1289\ J/(K \cdot kg)$ [68]. The tabulated data for the latent heat of water evaporation h_{evap} [66] was approximated with polynomial fit:

$$h_{evap} = \sum_{i=1}^{N} h_{evap,i} T^{i-1} \tag{46}$$

The coefficient values $a_{air,i}$, $a_{vap,i}$ and $h_{vap,i}$ for polynomial fits are listed in Tables 1–3, respectively. Finally, the vapour saturation pressure $p_{sat,vap}$ was evaluated according to [69]:

$$p_{sat,vap} = 611.21 \exp\left[\left(18.678 - \frac{T}{234.5}\right)\left(\frac{T}{257.14+T}\right)\right] \tag{47}$$

The unit of temperature for $p_{sat,vap}$ expression is °C.

3. Results and discussion

In this section, the experimental and modelling results are presented for the whole drying process; however, we are mainly concerned with predicting the drying rate during the constant-rate period with the proposed iterative method and CFD modelling. The constant-rate period by its length takes up a great part of the convective drying process of deep fixed beds [10], and predicting the drying rate during this period is of great importance.

Let us note that the convective drying rate evaluated from the heat power conservation equation for 100% outlet air relative humidity is the theoretical maximum drying rate, which can be achieved in the system with given inlet air conditions.

Table 1
Polynomial fit coefficients for the specific heat capacity of dry air.

i	$a_{air,i}$, $J/(kgK^i)$
1	$1.1159 \cdot 10^{3}$
2	$-1.7015 \cdot 10^{0}$
3	$1.1040 \cdot 10^{-2}$
4	$-3.8574 \cdot 10^{-5}$
5	$7.5225 \cdot 10^{-8}$
6	$-7.4782 \cdot 10^{-11}$
7	$2.9567 \cdot 10^{-14}$

3.1. Validation of the iterative method

The iterative method was validated by experimental data for two cases of biomass beds, namely, sawdust and barley.

In the sawdust drying case [13], the experimental and CFD numerical modelling data shown in Fig. 4 demonstrates that the outlet air relative humidity RH_{out} was constant with value of 100% during the whole constant-rate drying period, indicated by time interval [70; 350] min. During the same period, the reported experimental outlet air temperature was 32 ° C, while the experimental drying rate was 5 kg/h (the experimental drying rate here refers to the average value during the constant-rate period, which we evaluated from the experimental data provided in the drying rate time evolution figure from ref. [13]). However, in all performed sawdust experiments, the amounts of evaporated water calculated by mass balance were 10 ± 3.2% greater than the values obtained by weighting the bed before and after the drying process. Such disagreements indicate that the drying rate was calculated with a systematic error and; therefore, the approximate value of the actual lower limit of the drying rate in that case is 4.5 kg/h. Meanwhile, the iteratively estimated outlet air temperature was 32.75 ° C with drying rate value of 4.763 kg/h, which is within the experimentally measured range of [4.5,5] kg/h.

A comparison of the barley grain experimental drying rate over a 2-week period [19] with the iteratively estimated drying rate for the constant-rate period is shown in Fig. 5 (the term P_{sorp} was set to zero for drying rate estimation of barley grain). In this case, the constant-rate period is considered to be in the time interval of [0; 7] d, after which the mean drying rate began to fall. The severe fluctuations in the experimental data were explained by difficulties in accurately measuring small changes in a large grain load and imperfect control of the air temperature and humidity at the inlet. Nevertheless, the experimental outlet air temperature varied from 21.0 ° C to 21.3 ° C during constant-rate drying period with the average drying rate of 1.30 ± 0.15 kg/h, while the predictions of the iterative method were 20.5 ° C

Table 2
Polynomial fit coefficients for the specific heat capacity of water vapour.

i	$a_{vap,i}$, $J/(kgK^i)$
1	$-5.2458 \cdot 10^{3}$
2	$1.0390 \cdot 10^{2}$
3	$-6.0648 \cdot 10^{-1}$
4	$1.7676 \cdot 10^{-3}$
5	$-2.59480 \cdot 10^{-6}$
6	$1.5801 \cdot 10^{-9}$

Table 3
Polynomial fit coefficients for the latent heat of free water evaporation.

i	$h_{evap,i}$, $J/(kgK^{i-1})$
1	$8.0529 \cdot 10^{6}$
2	$-9.4702 \cdot 10^{4}$
3	$7.4657 \cdot 10^{2}$
4	$-3.3693 \cdot 10^{0}$
5	$9.1967 \cdot 10^{-3}$
6	$-1.5301 \cdot 10^{-5}$
7	$1.4742 \cdot 10^{-8}$
8	$-7.1074 \cdot 10^{-12}$
9	$1.0731 \cdot 10^{-15}$

and 1.27 *kg/h*. The experimental barley grain drying rate was calculated in the same way as in the case of sawdust. The iterative method's validation by both the sawdust and barley grain drying experiments is summarised in Table 4.

In addition, the beginning and the duration of the falling-rate period depends on the drying zone thickness and its movement speed through the bed. However, the heat power conservation equation (Eq. (1)) is valid independently of the of the drying zone thickness; therefore, it cannot be estimated with the iterative method. Consequently, the dynamics of the drying rate during the falling-rate period also cannot be captured by the iterative method, as it is clearly demonstrated in Fig. 5. Due to this important limitation, the iterative method is best suited to evaluate the convective drying characteristics for drying processes, in which the air is capable of reaching saturation within the bed for considerably long times (long constant-rate periods). This is usually achieved in beds with high bed thickness to drying zone thickness ratios. The cases in which the air is not able to reach saturation in the bed due to thin bed heights and non-uniform porosity distributions in beds are discussed in following sections.

3.2. Drying rate dependency on inlet air flow

Analysis of the drying rate q_{evap} an expression derived from the equation of the heat power conservation (given by Eq. (1)) leads to the conclusion that the drying rate q_{evap} is a linear function of inlet air mass flow rate q_{in} during the constant-rate drying period if the inlet air absolute humidity remains constant:

$$q_{evap} = k_{evap} q_{in} \tag{48}$$

where the slope coefficient k_{evap} is expressed from the governing equation of heat power conservation (Eqs. (1)) by substituting the equation terms (Eqs. (2), (8), (15), (19) and (20)):

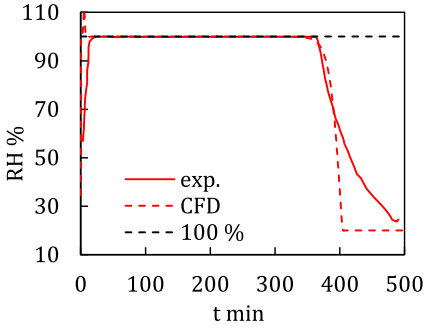

Fig. 4. Time evolution of the outlet air relative humidity in the sawdust drying experiment. Experimental data was taken from ref. [13].

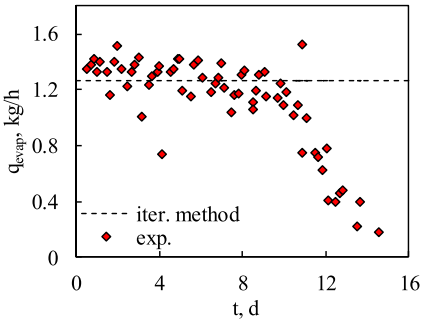

Fig. 5. Time evolution of the drying rate in the barley grain drying experiment. Experimental data was taken from ref. [19].

$$k_{evap} = \frac{\xi_{in,air} \int_{T_{out}}^{T_{in}} c_{p,air}(T)dT + (1 - \xi_{in,air}) \int_{T_{out}}^{T_{in}} c_{p,vap}(T)dT}{h_{evap}(T_{out}) + h_{sorp}(T_{out}) + h_{heat}(T_{out})} \tag{49}$$

Here, the mass fraction $\xi_{in,air} = q_{in,air}/q_{in}$ defines the inlet air absolute humidity. The term h_{sorp} is related to additional energy required to evaporate water below fibre saturation point and is defined as

$$h_{sorp}(T_{out}) = \frac{0.4 h_{evap}(T_{out}) \frac{(X_{m,fsp} - X_{m,end})^3}{3X_{m,fsp}^2}}{X_{m,0} - X_{m,end}} \tag{50}$$

and the term h_{heat} is related to the heating of dry solid material and the residual moisture content from T_{out} to T_{in}:

$$h_{heat}(T_{out}) = \frac{\int_{T_{out}}^{T_{in}} (c_{p,solid}(T) + X_{m,end} c_{p,water}(T))dT}{X_{m,0} - X_{m,end}} \tag{51}$$

Since the outlet air beyond the drying zone is fully saturated, it follows that the outlet air temperature T_{out} is independent of inlet air mass flow rate q_{in}. In addition, the drying rate expression given by Eqs. (48)–(51) shows that the drying rate of the deep fixed bed q_{evap} is also a function of the initial moisture content $X_{m,0} = m_{w,0}/m_s$ ($m_{w,0} = m_w(t = 0)$ is the initial water mass in the bed) but is not a function of the initial masses $m_{w,0}$ and m_s, which correspond to the total volume of the bed V_b. In other terms, the drying rate q_{evap} is independent of the bed volume V_b if the initial moisture content of the bed $X_{m,0}$ remains the same.

Notably, it is widely accepted by the researchers in the field to present their findings on biomass drying characteristics by using the concept of the moisture content [6,8,15,16,19,21,23,25–28,32,50]. However, using the moisture content defined as $X_m(t) = m_w(t)/m_s$ to characterise the convective drying process of the deep fixed beds during the constant-rate period does not seem a reasonable choice due to the following reasons. Firstly, the moisture content X_m describes the mass of water that is located within the whole bed volume at a specific time $m_w(t)$ disregarding the fact that the drying takes place only at the thin region of the bed, while the material is fully dry in the dried zone and fully wet at the wet-bulb zone (schematic illustration given in Fig. 1 c). Therefore, the moisture content X_m seems to be more suitable for thin beds, in which the drying zone thickness is greater than the bed thickness, and the drying takes place in the whole bed simultaneously. Secondly, the time evolution of moisture content $X_m(t)$ during the constant-rate period

$$X_m(t) = \frac{m_{w,0} - q_{evap} t}{m_s} \tag{52}$$

Table 4
Comparison of iterative method predictions with the fixed bed drying experiments of sawdust and barley grain.

	Sawdust experiment [13]	Iterative method	Barley grain experiment [19]	Iterative method
Inlet temperature T_{in}, ° C	57		25	
Inlet air mass flow rate q_{in}, kg/h	480.31		694.8	
Inlet air relative humidity RH_{in}, %	20		67	
Initial moisture content of fixed bed $X_{m,0}$	1.18		0.395	
Final moisture content of fixed bed $X_{m,end}$	0.056		0.175	
Outlet air temperature T_{out},°C	32	32.75	[21.0;21.3]	20.5
Drying rate q_{evap}, kg/h	[4.5;5.0]	4.763	1.30 ± 0.15	1.27

and its change rate

$$\frac{dX_m(t)}{dt} = -\frac{q_{evap}}{m_s} \tag{53}$$

are both dependent on the initial mass of the solid material m_s in the bed (and at the same time on bed volume) while the drying rate q_{evap} is not. Consequently, the drying results presented through $X_m(t)$ becomes directly incomparable for experiments with the same inlet air conditions but different bed volumes (for example, different bed heights) and cannot be generalised, especially when the initial masses $m_{w,0}$ and m_s are not explicitly reported.

3.3. Influence of the bed thickness on drying rate

The drying rate obtained from the heat power conservation equation is the theoretical maximum drying rate, which can be achieved only when the passing air is able to reach thermal equilibrium with the bed and relative humidity of 100% before leaving the bed. If these conditions are not satisfied during the drying process, the actual drying rate is lower than the iterative prediction. In the current and the following sections we will demonstrate two practical examples, which show how the 100% outlet air conditions could be unsatisfied.

Firstly, the air reaches saturation only when it passes through the drying zone. Therefore, the bed thickness should be greater than the drying zone thickness so that the air could reach the relative humidity of 100% before leaving the bed. One of the most important bed parameters that influence the thickness of the drying zone is the size of the bed particles. With decreasing particle size, the specific surface area and the rate of heat and mass transfer increase in the bed and, as a result, the air is able to reach saturation more rapidly and the drying zone becomes thinner. On the other hand, with increasing particle size, the effect of moisture and temperature intra-particle gradients becomes more prominent since it restricts water transport from interior parts to the particle surface, and the drying zone becomes thicker. This was confirmed by an experimental study by Lerman et al. [14], which showed that the drying zone thickness for woodchip biomass is significantly greater than for the sawdust biomass, which contains smaller particles than woodchips. It was also confirmed that the energy consumption for the convective drying process of biomass with smaller particles is lower [70], which is explained by the fact that with smaller particle sizes and, consequently, thinner drying zone, the duration of initial warm-up and falling-rate periods with lower drying efficiency decreases and, as result, the duration of more energetically efficient constant-rate period increases.

The CFD numerical modelling can be used to obtain outlet air parameters for wood chip beds with different thicknesses to demonstrate the influence of the bed thickness to the drying zone thickness ratio L_b/L_{dz} on the convective drying process. The configuration of the wood chip bed (except the bed thickness) and the inlet air conditions were the same as in the sawdust experiment. Furthermore, the drying zone thickness in the numerical simulation was defined as the distance in which the temperature inside the bed decreased from $T_{out} + 0.99(T_{in} - T_{out})$ to $T_{out} + 0.01(T_{in} - T_{out})$ at a given time and was measured to be $L_{dz} = 4.98\ cm$ for wood chips biomass (see Section 2.8).

The numerically obtained outlet air relative humidity when the bed thickness varied from $0.50L_{dz}$ to $1.50L_{dz}$ are shown in Fig. 6. In the numerical simulation, the drying zone thickness was defined as the distance in which the temperature inside the bed decreased from $T_{out} + 0.99(T_{in} - T_{out})$ to $T_{out} + 0.01(T_{in} - T_{out})$ at a given time and was measured to be $L_{dz} = 4.98\ cm$ for wood chips biomass. The results show that the outlet air reached 100% relative humidity during the constant-rate drying period only when the bed thickness L_b was greater than the drying zone thickness L_{dz}. In other cases, the outlet air was not saturated and; thus, the drying rate was lower than the iterative prediction.

3.4. Effects of enlarged porosity distribution near chamber walls

The lower drying rate than the theoretical maximum prediction by the iterative method can also be caused by inhomogeneity of porosity distribution, such as enlarged porosity distributions in the near-wall regions of the beds with larger biomass particle sizes. The air flow rates through such regions are higher than in the bulk region of biomass, causing uneven drying of the bed, where the near-wall regions dry out faster than the rest of the bed, as suggested by [21]. Since the part of the inlet air goes through the already dried regions near the chamber walls, the outlet air relative humidity could be below 100%.

The enlarged porosity is caused by wall effects on the particle packing efficiency near the walls. In fact, the porosity of wood chip biomass was experimentally measured to be a function of the distance from the bed wall with decreasing porosity values near the wall and approaching the bulk porosity value when the distance from the wall increases [63]. To illustrate the effect of enlarged porosity near the bed walls on the drying rate, we combined the discrete element method (DEM) results with the CFD numerical modelling [71,72].

Firstly, the DEM simulation of particle packing in a rectangular box (see Fig. 7) was performed to obtain the numerical porosity distribution for wood chip biomass bed. The wood chip particle shapes were approximated as spheres in DEM simulation with the same particle size distribution as the biomass used in experiments [63]. The DEM simulation results showed that porosity near the straight wall can be well approximated by a decreasing linear function. Assuming that the diameter of

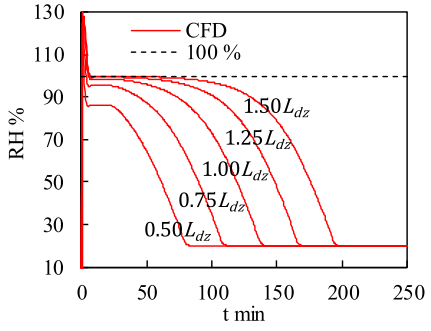

Fig. 6. Time evolution outlet air relative humidity with various bed thicknesses. The bed thickness is measured in terms of drying zone thickness.

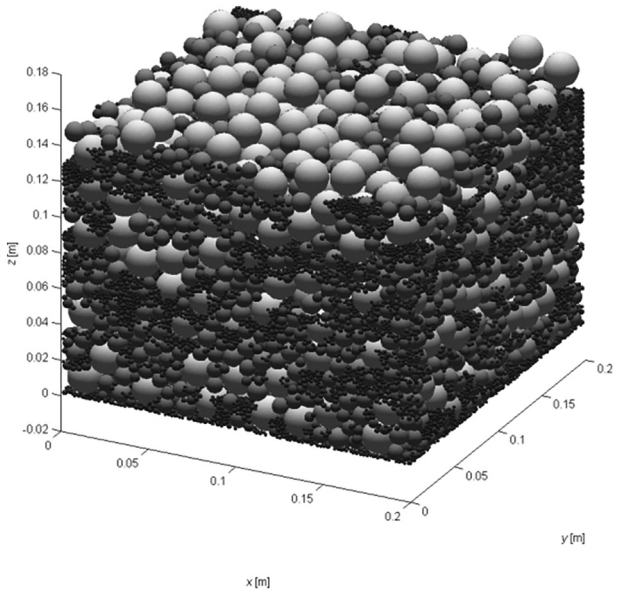

Fig. 7. DEM-simulated final state of the fixed bed containing wood chip particles approximated as spheres. Different colour intensities represent different particle sizes.

the cylindrical bed was sufficient, and the curvature of the bed did not affect the porosity, this function for the cylindrical coordinate system with axial symmetry can be written as:

$$\varepsilon = \begin{cases} \varepsilon_b & r \le (R_b - s_p) \\ \varepsilon_b + \dfrac{\varepsilon_w - \varepsilon_b}{s_p}\left(r - (R_b - s_p)\right) & r > (R_b - s_p) \end{cases} \quad (54)$$

where ε_b is the porosity of the bulk region, ε_w is the porosity at the wall (when $r = R_b$), s_p is the distance over which the wall has an effect on porosity, R_b is the diameter of the cylindrical fixed bed, and r is the distance from the symmetry axis of the bed.

The obtained porosity distribution function described by Eq. (54) was implemented in CFD numerical modelling with the following coefficient values: $\varepsilon_b = 0.28$, $\varepsilon_w = 0.9$ and $s_p = 3\ mm$. The bed height was also set to 20 *cm*. Otherwise, the CFD numerical modelling settings were left the same as in Section 3.3. The enlarged porosity region encompassed approximately 1.5% of the entire bed volume.

The CFD numerical modelling results with introduced enlarged porosity distribution (see Fig. 8) show that outlet air relative humidity reached 100% only for short period of time in the beginning of simulation and then it started to slowly decrease during the rest of the convective drying process. Consequently, the drying rate also decreased constantly during the convective drying without entering the constant-rate drying period. Such effect of enlarged porosity near the chamber walls might be more evident in smaller beds with larger biomass size fractions, where the near-wall region makes up a considerable part of the bed volume. In the general case, it should be considered before the iterative method is applied to evaluate the drying rate of the system.

4. Conclusions

In this paper, we propose a novel approach to describe the convective drying process of deep fixed porous material beds during the constant-rate drying period, which is based on the equation describing the heat power conservation within the drying zone. In addition, we propose a simple and fast iterative method to solve the equation since the conservation equation cannot be solved analytically due to nonlinear material property dependencies on temperature and the complex expressions of the equation terms. The proposed iterative method evaluates the outlet air temperature and the corresponding convective drying rate for any evaporating liquid from deep fixed porous material beds during a constant-rate drying period with given inlet air parameters. The validity of the proposed approach was examined against experimental and CFD numerical modelling data for two cases of biomass beds, namely, sawdust and barley grain.

The evaporation rate expression derived from the heat power conservation equation showed that the drying rate of deep fixed moist porous material bed is a linear function of the inlet air mass flow rate when inlet air absolute humidity is constant. Furthermore, the drying rate is a function of the initial moisture content of the bed; however, it is independent of the bed volume.

The CFD numerical modelling was used to illustrate the limits of approaches' applicability in cases when the bed thickness to drying zone thickness and enlarged porosity distribution near the bed walls affect the drying rate of the bed. Simulations showed that in beds in which the drying zone thickness is greater than the bed thickness, the heat and mass transport rate is insufficient for air to reach saturation before it exits the porous material bed. Furthermore, enlarged porosity near the bed walls causes higher flow rates of air in near-wall regions and changes the course of the drying: the relative humidity of the outlet air and the drying rate slowly decreases during the drying, and the drying process never enters the constant-rate drying period.

Overall, the presented novel approach evaluates the theoretical minimum possible outlet air temperature and theoretical maximum possible drying rate for a drying system with given inlet air conditions; therefore, it could be used as a fast, supplementary tool for evaluating the drying rate in various technological situations, designing industrial equipment and verifying the correctness of drying experiments, because it does not require the temporal and spatial discretization of the whole drying domain as in the sophisticated modelling approaches and can be implemented in any standard programming language without need of additional software.

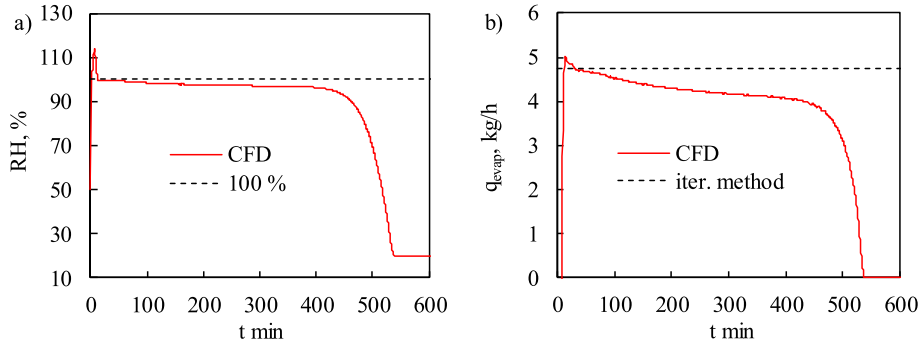

Fig. 8. Numerically obtained a) time evolution of outlet air relative humidity and b) time evolution of drying rate of wood chip bed with enlarged porosity distributions near the bed walls.

CRediT authorship contribution statement

Gediminas Skarbalius: Writing – original draft, Validation, Investigation, Formal analysis, Visualization. **Algis Džiugys:** Conceptualization, Methodology, Software, Supervision, Writing – review & editing. **Edgaras Misiulis:** Investigation, Formal analysis, Writing – review & editing. **Robertas Navakas:** Data curation, Writing – review & editing.

Declaration of Competing Interest

The authors declare that they have no known competing financial interests or personal relationships that could have appeared to influence the work reported in this paper.

Acknowledgements

This research was funded by the Research Council of Lithuania under project P-MIP-17-108 “ComDetect” (Agreement No. S-MIP-17-69), 2017-2020.

References

[1] S.R.H.B. Mark, D. Staples, Robert Malina, The limits of bioenergy for mitigating global life-cycle greenhouse gas emissions from fossil fuels, Nat. Energy (2017) https://doi.org/10.1038/nenergy.2016.202.
[2] W. Li, P. Ciais, D. Makowski, S. Peng, Data descriptor: a global yield dataset for major lignocellulosic bioenergy crops based on field measurements, Sci. Data. 5 (2018) 1–10, https://doi.org/10.1038/sdata.2018.169.
[3] F. Schwerz, D.D. Neto, B.O. Caron, C. Nardini, J. Sgarbossa, E. Eloy, A. Behling, E.F. Elli, K. Reichardt, Biomass and potential energy yield of perennial woody energy crops under reduced planting spacing, Renew. Energy 153 (2020) 1238–1250, https://doi.org/10.1016/j.renene.2020.02.074.
[4] J. Cai, Y. He, X. Yu, S.W. Banks, Y. Yang, X. Zhang, Y. Yu, R. Liu, A.V. Bridgwater, Review of physicochemical properties and analytical characterization of lignocellulosic biomass, Renew. Sust. Energ. Rev. 76 (2017) 309–322, https://doi.org/10.1016/j.rser.2017.03.072.
[5] S. Pang, A.S. Mujumdar, Drying of woody biomass for bioenergy: drying technologies and optimization for an integrated bioenergy plant, Dry. Technol. 28 (2010) 690–701, https://doi.org/10.1080/07373931003799236.
[6] L. Vorotinskienė, R. Paulauskas, K. Zakarauskas, R. Navakas, R. Skvorčinskienė, N. Striūgas, Parameters influencing wet biofuel drying during combustion in grate furnaces, Fuel. 265 (2020) https://doi.org/10.1016/j.fuel.2020.117013.
[7] S. Stenström, Drying of biofuels from the forest — a review, Dry. Technol. 35 (2017) 1167–1181, https://doi.org/10.1080/07373937.2016.1258571.
[8] T. Myllymaa, H. Holmberg, H. Hillamo, T. Laajalehto, P. Ahtila, Wood Chip drying in fixed beds drying kinetics and economics of drying at a municipal combined heat and power plant site, Dry. Technol. 3937 (2015) 205–215.
[9] A. Bryś, A. Kaleta, K. Górnicki, S. Głowacki, W. Tulej, J. Bryś, P. Wichowski, Some aspects of the modelling of thin-layer drying of sawdust, Energies. 14 (2021) 726, https://doi.org/10.3390/en14030726.
[10] P. Tanger, J.L. Field, C.E. Jahn, M.W. DeFoort, J.E. Leach, Biomass for thermochemical conversion: targets and challenges, front, Plant Sci. 4 (2013) 1–20, https://doi.org/10.3389/fpls.2013.00218.
[11] H. Rezaei, F. Yazdanpanah, C.J. Lim, S. Sokhansanj, Pelletization properties of refuse-derived fuel - effects of particle size and moisture content, Fuel Process. Technol. 205 (2020) 106437, https://doi.org/10.1016/j.fuproc.2020.106437.
[12] R. Adamski, D. Siuta, B. Kukfisz, P.T. Mitkowski, W. Szaferski, Influence of process parameters in superheated steam drying on fire and explosion parameters of woody biomass, Fuel Process. Technol. 211 (2021) 106597, https://doi.org/10.1016/j.fuproc.2020.106597.
[13] P. Bengtsson, Experimental analysis of low-temperature bed drying of wooden biomass particles, Dry. Technol. 26 (2008) 602–610, https://doi.org/10.1080/07373930801946726.
[14] P. Lerman, O. Wennberg, Experimental method for designing a biomass bed dryer, Biomass Bioenergy 35 (2011) S31–S39, https://doi.org/10.1016/j.biombioe.2011.04.033.
[15] J.K. Gigler, W.K.P. Van Loon, M.M. Vissers, G.P.A. Bot, Forced convective drying of willow chips, Biomass Bioenergy 19 (2000) 259–270, https://doi.org/10.1016/S0961-9534(00)00037-4.
[16] J. Zabski, P. Lampart, S. Gumkowski, Biomass drying: experimental and numerical investigations, Arch. Thermodyn. 39 (2018) 39–73, https://doi.org/10.1515/aoter-2018-0003.
[17] S. Pang, S. Bhattacharya, J. Yan, Drying of Biomass, Biosolids, and Coal: For Efficient Energy Supply and Environmental Benefits, 1st Editio, CRC Press Taylor & Francis Group, Cambridge, 2019.
[18] H.Y. Hiroaki Masuda, Ko Higashitani, Powder Technology: Handling and Operations, Process Instrumentation, and Working Hazards, 1st ed. CRC Press Taylor & Francis Group, 2019.
[19] P.J. Bowden, W.J. Lamond, E.A. Smith, Simulation of near-ambient grain drying: I. Comparison of simulations with experimental results, J. Agric. Eng. Res. 28 (1983) 279–300, https://doi.org/10.1016/0021-8634(83)90062-8.
[20] G.V. Kuznetsov, S.V. Syrodoy, N.A. Nigay, V.I. Maksimov, N.Y. Gutareva, Features of the processes of heat and mass transfer when drying a large thickness layer of wood biomass, Renew. Energy 169 (2021) 498–511, https://doi.org/10.1016/j.renene.2020.12.137.
[21] L. Vorotinskienė, Parameters affecting biomass drying during combustion in moving grate furnaces, Energetika. 65 (2019) 74–84, https://doi.org/10.6001/energetika.v65i1.3976.
[22] T. Myllymaa, H. Holmberg, H. Hillamo, T. Laajalehto, P. Ahtila, Wood Chip drying in fixed beds: drying kinetics and economics of drying at a municipal combined heat and power plant site, Dry. Technol. An Int. J. 33 (2014) 37–41, https://doi.org/10.1080/07373937.2014.945179.
[23] H. Rezaei, C.J. Lim, A. Lau, X. Bi, S. Sokhansanj, Development of empirical drying correlations for ground wood chip and ground wood pellet particles, Dry. Technol. 35 (2017) 1423–1432, https://doi.org/10.1080/07373937.2016.1198912.
[24] K.R. Subahana, R. Natarajan, Theoretical modelling and experimental investigation of the convective drying kinetics of biomass in an improved solar tunnel dryer, Biofuels. 10 (2019) 279–286, https://doi.org/10.1080/17597269.2015.1132372.
[25] H. Holmberg, P. Ahtila, O. Ahtila, Experimental study on drying of bark in fixed beds, Dry. Technol. 29 (2011) 953–960, https://doi.org/10.1080/07373937.2010.551305.
[26] H. Li, Q. Chen, X. Zhang, K.N. Finney, V.N. Sharifi, J. Swithenbank, Evaluation of a biomass drying process using waste heat from process industries: a case study, Appl. Therm. Eng. 35 (2012) 71–80, https://doi.org/10.1016/j.applthermaleng.2011.10.009.
[27] P.S.T. Sai, Drying of solids in a rotary dryer, Dry. Technol. 31 (2013) 213–223, https://doi.org/10.1080/07373937.2012.711406.
[28] S. Danielsson, A. Rasmuson, The influence of drying medium, temperature, and time on the release of monoterpenes during convective drying of wood chips, Dry. Technol. 20 (2002) 1427–1444, https://doi.org/10.1081/DRT-120005860.
[29] T. Hosseini, L. Zhang, Process modeling and techno-economic analysis of a solar thermal aided low-rank coal drying-pyrolysis process, Fuel Process. Technol. 220 (2021), 106896https://doi.org/10.1016/j.fuproc.2021.106896.
[30] K. Xu, M. Zhang, R. Ju, A.S. Mujumdar, Y. Liu, Effect of different drying methods on the characteristics of chicken powder added with basil during storage, Dry. Technol. 0 (2021) 1–10, https://doi.org/10.1080/07373937.2021.1908344.
[31] F.N.C. de Almeida, G. Johann, N.W. Siqueira, G.K. Souza, N.C. Pereira, Convective drying of *Moringa oleifera* seeds: kinetics modelling and effects on oil yield from different extraction techniques, Biomass Convers. Biorefin. (2021), https://doi.org/10.1007/s13399-020-01198-8.
[32] M.L. Hoang, P. Verboven, M. Baelmans, A continuum model for airflow, heat and mass transfer in bulk of chicory roots, Am. Soc. Agric. Biol. Eng. 46 (2003) 1603–1611.
[33] B. Acoglu, P. Yolci Omeroglu, The effect of drying processes on pesticide residues in orange (*Citrus sinensis*), Dry. Technol. 0 (2021) 1–16, https://doi.org/10.1080/07373937.2021.1946078.
[34] N.S. Bhatkar, S.S. Shirkole, A.S. Mujumdar, B.N. Thorat, Drying of tomatoes and tomato processing waste: a critical review of the quality aspects, Dry. Technol. 0 (2021) 1–25, https://doi.org/10.1080/07373937.2021.1910832.
[35] M. Stramarkou, S. Papadaki, K. Kyriakopoulou, I. Tzovenis, M. Chronis, M. Krokida, Comparative analysis of different drying techniques based on the qualitative characteristics of Spirulina platensis biomass, J. Aquat. Food Prod. Technol. 30 (2021) 498–516, https://doi.org/10.1080/10498850.2021.1900969.
[36] S. Cheng, W. Su, L. Yuan, M. Tan, Recent developments of drying techniques for aquatic products: with emphasis on drying process monitoring with innovative methods, Dry. Technol. 0 (2021) 1–18, https://doi.org/10.1080/07373937.2021.1895205.
[37] B. El Fil, S. Garimella, The state of the art in energy saving techniques for garment/textile drying, Dry. Technol. 0 (2021) 1–16, https://doi.org/10.1080/07373937.2021.1938599.
[38] E. McEwen, J.R. O'Callaghan, Through drying of deep beds of wheat grain, Eng. 10 (1954) 817–819.
[39] Grain drying, in: W.V. Hukill, J.A. Anderson, A.W. Alcock (Eds.), Storage Cereal Grain their Prod, Association Cereal Chemist, 1954.
[40] A.W. Aregba, J.P. Nadeau, Comparison of two non-equilibrium models for static grain deep-bed drying by numerical simulations, J. Food Eng. 78 (2007) 1174–1187, https://doi.org/10.1016/j.jfoodeng.2005.12.030.
[41] M. Hemis, C.B. Singh, D.S. Jayas, A. Bettahar, Simulation of coupled heat and mass transfer in granular porous media: application to the drying of wheat, Dry. Technol. 29 (2011) 1267–1272, https://doi.org/10.1080/07373937.2011.591712.
[42] A.A. Satimehin, A mathematical model for deep bed drying of gelatinized white yam, Int. J. Energy Eng. 4 (2A) (2014) 33–39, https://doi.org/10.5923/j.ijee.201401.05.
[43] B.K. Bala, Deep-Bed and Continuous Flow Drying, Second Edi, John Wiley & Sons, West Sussex, 2017.
[44] D. Zare, D.S. Jayas, C.B. Singh, A generalized dimensionless model for deep bed drying of Paddy, Dry. Technol. 30 (2012) 44–51, https://doi.org/10.1080/07373937.2011.615429.
[45] J.R. Sharp, A review of low temperature drying simulation models, J. Agric. Eng. Res. 27 (1982) 169–190, https://doi.org/10.1016/0021-8634(82)90060-9.
[46] J.L. Parry, Mathematical modelling and computer simulation of heat and mass transfer in agricultural grain drying: a review, J. Agric. Eng. Res. 32 (1985) 1–29, https://doi.org/10.1016/0021-8634(85)90116-7.
[47] S. Pabis, D.S. Jayas, Deep-bed grain drying - a review of particular theories, Dry. Technol. 11 (1993) 1553–1582, https://doi.org/10.1080/07373939308916919.

[48] A.S. Mujumdar, Basic process calculations and simulations in drying, Handb. Ind. Dry. CRC Press, Boca Raton 2021, p. 2006, https://doi.org/10.1201/9781420017618.
[49] R.P. Ramachandran, M. Akbarzadeh, J. Paliwal, S. Cenkowski, Computational fluid dynamics in drying process modelling—a technical review, Food Bioprocess Technol. 11 (2018) 271–292, https://doi.org/10.1007/s11947-017-2040-y.
[50] M. Huttunen, A. Holmberg, S. Stenström, Modeling fixed-bed drying of bark, Dry. Technol. 35 (2017) 97–107.
[51] A. Shomali, B.A. Souraki, Experimental investigation and mathematical modeling of drying of green tea leaves in a multi-tray cabinet dryer, Heat Mass Transf. (2019) 3645–3659, https://doi.org/10.1007/s00231-019-02662-6.
[52] D.I.S. Silva, G.F.M.V. Souza, M.A.S. Barrozo, Heat and mass transfer of fruit residues in a fixed bed dryer: modeling and product quality, Dry. Technol. 37 (2019) 1321–1327, https://doi.org/10.1080/07373937.2018.1498509.
[53] J. Yrjölä, J.J. Saastamoinen, Modelling and practical operation results of a dryer for wood chips, Dry. Technol. 3937 (2006) https://doi.org/10.1081/DRT-120004041.
[54] S. Pang, Q. Xu, Drying of Woody Biomass for Bioenergy Using Packed Moving Bed Dryer: Mathematical Modeling and Optimization Drying of Woody Biomass for Bioenergy Using Packed Moving Bed Dryer: Mathematical Modeling and Optimization, 3937, 2010 https://doi.org/10.1080/07373931003799251.
[55] B. Peters, E. Schröder, C. Bruch, T. Nussbaumer, Measurements and particle resolved modelling of heat-up and drying of a packed bed, Biomass Bioenergy 23 (2002) 291–306.
[56] Z.H. Wang, G. Chen, Heat and mass transfer in fixed-bed drying, Chem. Eng. Sci. 54 (1999) 4233–4243, https://doi.org/10.1016/S0009-2509(99)00118-9.
[57] J.J. Wang, Mathematical modeling of the drying process in a fixed–bed dryer, Numer. Heat Transf. Part B Fundam. (2007) 37–41, https://doi.org/10.1080/10407799308955891.
[58] A. Khouya, Modelling and analysis of a hybrid solar dryer for woody biomass, Energy. 216 (2021) 119287, https://doi.org/10.1016/j.energy.2020.119287.
[59] S.L.Z. Samuel, V. Glass, Wood Handbook, Chapter 04: Moisture Relations and Physical Properties of Wood, 2010.
[60] S.L. Zelinka, S.V. Glass, J.E. Jakes, D.S. Stone, A solution thermodynamics definition of the fiber saturation point and the derivation of a wood–water phase (state) diagram, Wood Sci. Technol. 50 (2016) 443–462, https://doi.org/10.1007/s00226-015-0788-7.
[61] COMSOL, Multiphysics®, v. 5.1, www.comsol.com 2020.
[62] L. Durlofsky, J.F. Brady, Analysis of the brinkman equation as a model for flow in porous media, Phys. Fluids 30 (1987) 3329–3341, https://doi.org/10.1063/1.866465.
[63] S. Hamel, W. Krumm, Near-wall porosity characteristics of fixed beds packed with wood chips, Powder Technol. 188 (2008) 55–63, https://doi.org/10.1016/j.powtec.2008.03.011.
[64] M. Bellais, Modelling of the Pyrolysis of Large Wood Particles, KTH - Royal Institute of Technology, 2007 https://www.diva-portal.org/smash/record.jsf?pid=diva2%3A12258&dswid=-9293.
[65] A. Singhal, S. Cloete, S. Radl, R. Quinta-ferreira, S. Amini, Heat transfer to a gas from densely packed beds of cylindrical particles, Chem. Eng. Sci. 172 (2017) 1–12.
[66] T.J.B.W.M. Haynes, David R. Lide, CRC Handbook of Chemistry and Physics, 97th ed. CRC Press Taylor & Francis Group, 2016.
[67] İ. Dinçer, C. Zamfirescu, Drying Phenomena: Theory and Applications, John Wiley & Sons, 2015 https://doi.org/10.1002/9781118534892.
[68] Y. Sun, C.C. Pantelides, Z.S. Chalabi, Mathematical modelling and simulation of near-ambient grain drying, Comput. Electron. Agric. 13 (1995) 243–271, https://doi.org/10.1016/0168-1699(95)00018-Y.
[69] A.L. Buck, New equations for computing vapor pressure and enhancement factor, J. Appl. Meteorol. Climatol. 20 (1981) 1527–1532, https://doi.org/10.1175/1520-0450(1981)020<1527:NEFCVP>2.0.CO;2.
[70] L. Fiorineschi, G. Cascini, F. Rotini, A. Tonarelli, Versatile grinder technology for the production of wood biofuels, Fuel Process. Technol. 197 (2020) 106217, https://doi.org/10.1016/j.fuproc.2019.106217.
[71] A. Džiugys, R. Navakas, The role of friction in mixing and segregation of granular material, Granul. Matter 11 (2009) 403–416, https://doi.org/10.1007/s10035-009-0145-3.
[72] R. Navakas, A. Džiugys, B. Peters, A community-detection based approach to identification of inhomogeneities in granular matter, Phys. A Stat. Mech. Appl. 407 (2014) 312–331, https://doi.org/10.1016/j.physa.2014.04.003.